Simulation of the structure and mechanics of crystalline 4,4#-diphenylmethane diisocyanate (MDI) with n -butanediol (BDO) as chain extender

Simulation of the structure and mechanics of crystalline 4,4'-diphenylmethane diisocyanate (MDI) with n-butanediol (BDO) as chain extender

Nikolaos Lempesis[(a)], Pieter J. in 't Veld[(b)], Gregory C. Rutledge[(a)]

(a) Department of Chemical Engineering, Massachusetts Institute of Technology, 77 Massachusetts Avenue, Cambridge, Massachusetts 02139, United States

(b) BASF SE, Polymer Physics, 38 Carl-Bosch street, Ludwigshafen D-67056, Germany

Abstract: We report molecular simulation at the atomistic level of crystalline 4,4'-diphenylmethane diisocyanate (MDI) with n-butanediol (BDO) as chain extender, henceforth denoted as MDI/BDO, which is one of the most important components of thermoplastic polyurethanes. This work studies the structure and properties of crystalline MDI/BDO at equilibrium and under deformation. An atomistic molecular model of the MDI/BDO unit cell was constructed from fractional coordinates available for related model compounds and space group symmetry, and bulk properties of the subsequently equilibrated crystal were estimated by molecular dynamics. Overall stress-strain behavior of the crystal to small strains was simulated at different strain rates. The full stiffness matrix of crystalline MDI/BDO was extracted, allowing for the complete characterization of the linear elastic behavior of the crystal.

1. Introduction

The term “thermoplastic polyurethanes” encompasses a broad family of polymeric materials with growing practical utility and commercial interest. From a scientific standpoint, these materials are of great importance, because they constitute multiphase, heterogeneous block copolymers having complicated constituent parts, in terms of chemistry and morphology. In general, thermoplastic polyurethanes are composed of relatively ordered and organized aggregates of species A interspersed at random orientations within a less ordered polymer matrix of species B. The two species, A and B, are chemically bonded to each other. In the literature, the organized aggregates are usually referred to as the “hard component”, whereas the less organized polymer matrix is called the “soft component”. These designations are empirical and stem from the response of these components to mechanical deformation.

In all thermoplastic polyurethanes, the hard component consists of a first segment containing urethane bonds, which is connected to a second segment known as the chain extender. In many thermoplastic polyurethanes, the first constituent is diphenylmethane 4,4’-diisocyanate (MDI) and the chain extender is 1,4-butanediol (BDO). These two segments, chemically connected to each other, constitute the hard component of some commercially important thermoplastic polyurethanes[1] and will be denoted henceforth as MDI/BDO. The chemical structure of the MDI/BDO repeating unit is shown in Figure 1(a).

Over the past decades, the structure, geometry and overall morphology of the crystalline MDI/BDO segment have been extensively studied. The idea that neighboring polymer chains of the hard component of polyurethanes are held together by hydrogen bonds was first suggested by Schollenberger and coworkers[2] in 1962. However, it was not until 1966 that Cooper and Tobolsky[3] reported experimental evidence that polyurethanes indeed compose a two phase structure consisting of high modulus domains (hard segments or hard

components) interspersed within a rubbery matrix (soft segment or soft component) and held together by “secondary forces of valence nature”. Since then, extensive efforts by Bonart et al[4-7] and others[8-13] have led to a much greater understanding of the physical and geometrical structure of these materials. Bonart et al[6, 7] employed wide angle x-ray investigations to determine the arrangement of atoms within the hard segment layers in urethane elastomers having BDO as chain extender to understand better the hydrogen bonding between MDI/BDO segments of neighboring chains. They concluded that the formation of hydrogen bridges is only possible between the oxygen atom of the carbonyl group >C=O of one chain and the hydrogen of the amine group >N-H of a neighboring chain. A few years later, refinement of X-ray diffraction evidence[9, 12, 14] led to a proposed packing of the chains of the polyurethane elastomer in three dimensional space.

In this work, we report the use of computational modeling and molecular simulations to validate and extend existing knowledge on the three-dimensional structure of the MDI/BDO unit cell, for which there is still ambiguity and contradiction in the experimental record. Attention is given to the construction of an atomistic model from basic principles. In preparation for simulation of the crystalline MDI/BDO system, we first built the perfect crystal by replicating the constructed unit cell in three-dimensional space. This report is organized as follows. Section 2 describes the materials and the process of constructing our atomistic model crystal. In Section 3.1, we describe the methods used to validate a force field by estimating equilibrium crystal properties and comparing them to available experimental data, whereas in Section 3.2, our strategy to conduct nonequilibrium deformation simulations is discussed. Our findings for both equilibrium and deformation simulations are reported and discussed in Sections 4.1 and 4.2 respectively. Finally, Section 5 summarizes the basic conclusions of this work.

2. Materials

2.1 Crystal structure

Initially, a triclinic unit cell was proposed for the crystalline structure of the hard segment[9] based on the structure of the model compound methanol-capped MDI (MeMMe*) having dimensions: a = 5.2 Å, b = 4.8 Å, c = 35.0 Å, $\alpha = 115^{o}$, $\beta = 121^{o}$ and $\gamma = 85^{o}$. The space group was $P_{\bar{1}}$ and the unit cell contained two repeating (asymmetric) units of a single chain. However, the proposed unit cell predicted a very high crystalline density $\rho_{crystal} = 1.58$ g/cm^3. In an effort to improve upon that initial work, Blackwell et al[15] proposed a slightly modified triclinic unit cell for the polyurethane hard segment comprising MDI/BDO, having lattice parameters: a = 5.05 Å, b = 4.67 Å, c = 37.9 Å, $\alpha = 116^{o}$, $\beta = 116^{o}$ and $\gamma = 83.5^{o}$, with a lower, albeit still high, crystalline density of $\rho_{crystal} = 1.45$ g/cm^3. Both of these densities were in clear disagreement with all known experimentally measured crystalline densities of polyurethanes having crystalline MDI/BDO as hard segment[16, 17]. The experimentally measured crystalline density for these structures amounted to approximately $\rho_{crystal}^{exp} = 1.31 \pm 0.01$ g/cm^3; the uncertainty in the experimental density reflects the deviation in values reported by different research groups[16, 17]. Finally, Born et al[17] proposed a triclinic unit cell for a model compound of MDI/BDO, complete with fractional coordinates, that complied with the experimental density observations.

The atomistic molecular model of the triclinic MDI/BDO unit cell used in this work was built based on the fractional coordinates of the model compound studied by Born et al[17]. The asymmetric unit of this molecule contained atoms 8 through 27 of the MDI/BDO asymmetric unit depicted in Figure 1(b). The lacking fractional coordinates of atoms 1-7 were calculated by exploiting the symmetry of the MDI/BDO unit. In particular, the missing atoms 1-7 were assumed to have the same relation to atom 8, as atoms 21-27 have to atom 18. To

reproduce the missing atoms, we constructed them one by one starting off from atom 8 and calculated them based on the geometry and orientation characteristics of the already known atom group 21-27. For example, atom 6 is the nitrogen atom of the urethane group and is connected to the phenyl ring carbon atom 8. The distance r of the bond between atoms 8 and 6 is already known from the bond distance between atoms 18 and 21. Therefore, atom 6 should lie on a spherical locus having atom 8 at its center and radius r. To determine the exact location of atom 6 on that spherical shell, the orientation is needed. This was given by the azimuthal and polar angles of atom 6 with respect to an orthonormal reference system having at its origin atom 8. These two angles were given by the angles formed among atoms 6, 8, 13 and 6, 8, 11 respectively and were identical to those formed by atoms 21, 18, 19 and 21, 18 and 15. In an analogous way, the fractional coordinates of the rest of the missing atoms of the asymmetric MDI/BDO unit were calculated. Thus obtained, the starting fractional coordinates of the entire MDI/BDO unit cell are reported in Appendix A of the Supporting Information.

The resulting triclinic unit cell includes two asymmetric units in a single chain and has the following lattice parameters: a = 4.92 Å, b = 5.66 Å, c = 38.35 Å, $\alpha = 124^{o}$, $\beta = 104.5^{o}$ and $\gamma = 86^{o}$. Two dimensional projections of this unit cell are shown in Figure 1(c) and 1(d). In this figure, the c-crystallographic axis has been aligned with the z-Cartesian axis. Figure 1(d) shows a representation of the conformation of two neighboring chains in the lattice in this model crystal. Hydrogen bonds are formed between the N–H group of one chain and the oxygen atom of the carbonyl group of the neighboring chain. The chain alignment of our model compares favorably to related experimental observations regarding the three dimensional arrangement of hard segment chains[4, 6, 18].

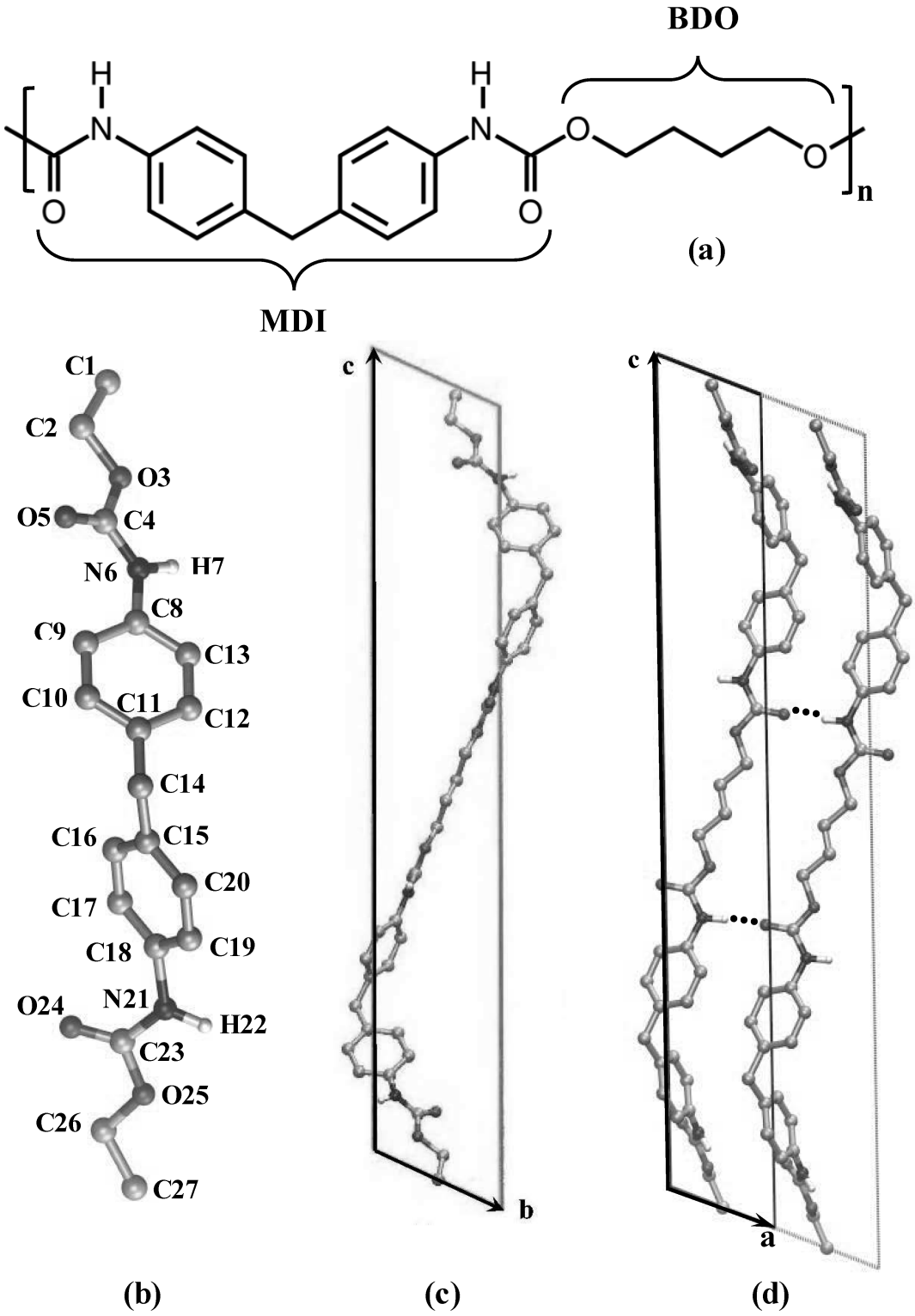

Figure 1: (a) Chemical formula of the MDI/BDO repeat unit. Atom enumeration of the MDI/BDO asymmetric unit and unit cell projections along the: (b) a- and (c) b-crystallographic axis of crystalline MDI/BDO. In part (c), two neighboring unit cells along the a-axis are shown to illustrate the formation of hydrogen bonds, depicted with three black

dots. Atom types are distinguished by character and number: CH_n groups (C#); oxygen (O#); nitrogen (N#); hydrogen attached to nitrogen (H#).

To create the crystalline model of MDI/BDO for simulation, the unit cell of Figure 1 was replicated in the a, b and c-directions, for a total of (9 x 8 x 5) unit cells and a total size of 4.428 x 5.166 x 19.175 nm, containing 72 chains of 270 sites each, for a total of 19440 sites in the simulation box.

Patterson and coworkers[18] performed a conformational analysis for the MDI/BDO crystal structure. They based their research on the conformation energy of various possible chain alignments. More precisely, they found that there are two stable structural configurations for the hard segment crystal. Two distinct types of spherulites were visible in optical micrographs and diffraction experiments. Type I spherulites showed no visible birefringence, while type II exhibited the classic Maltese cross extinction pattern. Furthermore, the conformational analysis of these two types of crystal structures done by Patterson et al.[18] showed that polymer chains in the type II crystal structure assumed minimum energy configurations and close packing to form a highly ordered array, as opposed to the type I crystal structure, which were believed to be distorted and paracrystalline in nature. They proposed that the first crystal structure formed a double helix with only van der Waals interactions between the two MDI/BDO chains of the double-helix, while the second type formed hydrogen bonds between neighboring MDI/BDO chains. The results of their study were in accordance with other experimental studies investigating polymorphism of crystalline MDI/BDO structures in polyurethanes[19-24]. The structures depicted in Figure 1 are closer to the denser structure characteristic of Type II, which corresponds to the hydrogen bonded conformation[18]. As Figure 1(d) shows, two hydrogen bonds are formed in the ac-

plane between chains in two neighboring unit cells, for a total of two hydrogen bonds per unit cell. This trait of our model is in excellent agreement with related experimental observations[4, 6].

3. Methods

3.1 Equilibrium molecular dynamics (MD) simulations

Three replicas of crystalline MDI/BDO were created based on the lattice details mentioned in Section 2. In the process, we have made sure that the atomistic models conformed to the chemical, structural and geometrical requirements of the unit cell proposed by Born et al[17]. The three atomistic crystal structures were then used as initial configurations and equilibrated by molecular dynamics simulations using LAMMPS[25] in the NPT statistical ensemble at T = 300 K and P = 1 atm, far below the experimentally observed softening temperature T_m = 503 – 513 K [6, 15, 26] of the MDI/BDO hard component at atmospheric pressure. The force field used in this work was based on previous investigations of molecules containing urethane bonds and polyol segments. Therein, harmonic bond stretching and bending potentials were used, along with a harmonic improper potential to maintain the planarity of the phenyl ring and of the overall structure of the urethane bond. The non-bonded Lennard-Jones parameters, as well as some of the bond bending contributions, were taken from a slight modification of the TraPPE-united atom (UA) force field[27-32]. Parameters for torsional and Coulombic contributions to the total potential energy were taken from the OPLS-UA force field or some recent modifications of it[33-45]. Originally, the conventional OPLS-UA force field was tested, but it failed to reproduce the target density and lattice structure. For this reason, the TraPPE-UA parameters for Lennard-Jones interactions (only) were substituted in their entirety, with satisfactory results; in implementing the TraPPE-UA interactions, intramolecular 1-4 interactions were explicitly excluded from calculation. The interaction parameters of the force field, as well as

the functional forms for the quantification of inter- and intramolecular interactions, are listed in Appendix B of the Supporting Information.

The time step for molecular dynamics simulation was 2 fs. The Velocity Verlet method[46] was used to integrate the equations of motion. The deterministic Nose-Hoover thermostat and barostat were used to maintain isothermal and isobaric conditions in the system[47, 48], with time constants of 100 and 1000 fs, respectively. In crystal lattice simulations, atomic displacements are due predominantly to fast vibrational motions, so crystal systems tend to equilibrate rapidly (< 1-2 ns) and sample phase space efficiently. Each simulation ran for a total of 20 ns, the last 15 ns of which were sampled every 500 fs for the calculation of ensemble averages. All simulations were run in triplicate.

3.2 Deformation analysis

The three constructed crystal configurations were subjected to a series of deformation simulations to assess the deformation mechanics of crystalline MDI/BDO. Prior to imposition of deformation, all configurations were equilibrated using MD in the NσT ensemble for 5 ns. MD simulations in the NσT ensemble were realized by using the conventional "fix npt" command of LAMMPS and allowing the six independent components of the simulation box tensor to change independently. This step ensured that all three principal elements of the stress tensor were equal to about 1 atm, and that all off-diagonal elements were close to zero. As in the case of equilibrium MD simulation (Section 3.1), the deterministic Nose-Hoover thermostat and barostat were used to maintain isothermal and isobaric conditions in the system[47, 48], but with time constants of 100 fs for both.

As was done previously for simulations of crystalline and semicrystalline poly(tetramethylene oxide) (PTMO)[49], simple strain deformations were performed using a non-steady-state, non-equilibrium form of molecular dynamics in which each crystalline

specimen was deformed by changing one component of the strain tensor, at a constant strain rate $\dot{\varepsilon} = 5 \times 10^6\ s^{-1}$, up to a true strain of $\varepsilon = 0.1$, while the other components were held constant at their equilibrium values. The full elastic stiffness tensor **C** was then extracted from the slopes of the stress-strain curves at small strain[50, 51]. The elastic compliance tensor $\mathbf{S} = \mathbf{C}^{-1}$ was then calculated. The elastic moduli of crystalline MDI/BDO were finally expressed as the inverses of the diagonal elements of the compliance tensor[52] (in Voigt notation), $E_i = 1/S_{ii}$, i=1,2,3 and $G_{i-3} = 1/S_{ii}$, i=4,5,6. Additionally, the elements of the compliance tensor have been used to estimate the isothermal compressibility $\beta_T = \left[S_{11} + S_{22} + S_{33} + 3\left(S_{12} + S_{23} + S_{13}\right)\right]$ and the bulk modulus $K = \beta_T^{-1}$.

In addition to the simple strain deformations, uniaxial extension was also considered. In this type of loading condition, the system was deformed in one of the three principal directions, while allowing the two lateral dimensions to change in response to the barostat in those directions[53], so that a constant stress at about 1 atm was maintained. These types of deformation yielded independent estimates of the elastic (Young's) moduli, E_i, and isothermal compressibility, β_T, directly, and served as checks on the numerical accuracy of the first deformation method (simple strain), which is itself complete. All deformations were realized at constant deformation rate $\dot{\varepsilon} = 5 \times 10^6\ s^{-1}$. As before, the time step was 2 fs, and the Velocity Verlet method was used to integrate the equations of motion. The deformation ran for 3×10^7 steps. The Nose-Hoover thermostat was used to remove the thermal energy arising from deformation and ensure isothermal conditions; for thermal conductivities typical of organic crystals, the rise in temperature for a deforming sample size on the order of the simulation box is expected to be negligible. Here also, simulations were run in triplicate.

4. Results and Discussion

4.1 Equilibrium crystal properties

During the course of the equilibrium MD simulations, the dimensions of the simulation box were free to change. After the completion of this set of runs, the equilibrium crystal density was calculated from the time averages of the triplicate runs. The results are summarized in Table 1. Not only the density, but also the individual lattice parameters compare favorably to the experimentally reported crystal density and lattice parameters. These results confirm the stability and accuracy of the proposed MDI/BDO atomistic model under the action of the proposed force field.

Table 1: Comparison of simulated equilibrium density and lattice parameters with the corresponding experimental values for crystalline MDI/BDO.

	Simulation	**Experiment**	**Ref.**
Crystal density (g/cm^3)	1.31 ± 0.02	1.31 ± 0.01	[16, 17]
a (nm)	0.494 ± 0.020	0.492	[17]
b (nm)	0.574 ± 0.020	0.566	[17]
c (nm)	3.803 ± 0.050	3.835	[17]
α (deg)	122.3 ± 2.1	124	[17]
β (deg)	105.06 ± 1.95	104.5	[17]
γ (deg)	87.3 ± 1.72	86	[17]

As an extra level of validation of the structure of the considered model crystal, but also of the selected force field, the static structure factor S(q) was calculated and compared to available experimental[14, 17] and computational results[18]. The static structure factor S(q) was calculated with the help of equation 1:

$$S(\mathbf{q}) \propto \frac{1}{N}\left\langle \sum_{i,j} \exp\left[i\mathbf{q}\cdot\left(\mathbf{r}_i - \mathbf{r}_j\right)\right]\right\rangle \quad (1)$$

In equation 1, the angular brackets denote averaging over the entire ensemble of pairs of atoms i and j and **q** is the wave vector, which is connected to the d-spacing via $\mathbf{q} = \frac{2\pi}{\mathbf{r}}$.

The calculated static structure factor S(q) for the MDI/BDO crystal is shown in figure 2. Comparison of this structure factor to the location of peaks in the experimental X-ray diffraction measurements, indicated as dotted lines in Figure 2, confirms agreement between the experimentally measured structure and the computationally predicted one. The corresponding d-spacings calculated via simulations and measured by X-ray experiments are indexed and compared in Table 2. In Figure 2, we show that our simulation results provided very subtle diffraction peaks for (001), (002) and (003) which are not observed in experiment (no dotted lines are drawn); however, these peaks are calculated to be almost thirty five times weaker than the experimentally observed (004) peak. In addition to that, the conformational analysis of the MDI/BDO crystal structure implemented by Patterson et al[18], in which the hydrogen-bonded conformation for the MDI/BDO segments was the same as that used in this work, provided very weak diffraction peaks for these three Miller index sets. Hence, it can be concluded that the constructed atomistic MDI/BDO model describes well the structure of the actual crystal and, by extension, the force field captures accurately the inter- and intramolecular interactions.

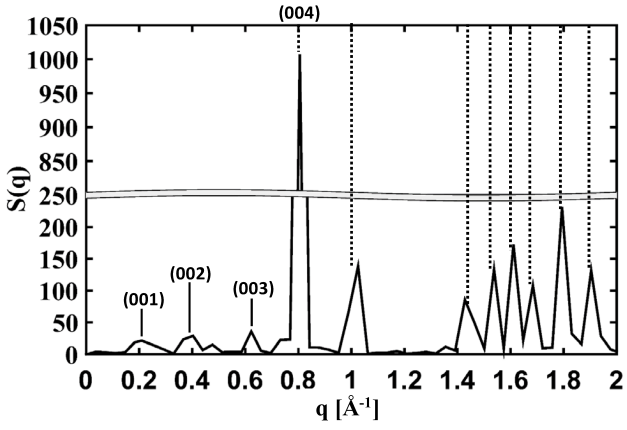

Figure 2: Static structure factor calculated for the perfect MDI/BDO crystal at small wave vector **q** values. The dotted lines indicate the position of the experimental peaks where applicable.

Table 2: Comparison between experimentally measured [14, 17] and simulated d-spacing distances for the MDI/BDO crystal. (*) d_{exp} values are taken from conformational analysis[18].

Miller Indices	d_{exp} [Å]	d_{sim} [Å]
(001)*	32.1	32.5
(002)*	16.0	15.8
(003)*	10.7	10.3
(004)	7.7	7.8
(005)	6.4	6.2
$(0\bar{1}1)$	4.1	4.1
$(0\bar{1}3)$	3.9	3.9
$(0\bar{1}4)$	3.8	3.7
(015)	3.3	3.3
$(\bar{1}02)$	4.3	4.4
$(\bar{1}05)$	3.5	3.4

4.2 Linear elasticity of crystalline MDI/BDO

Figure 3 shows the 36 averaged stress-strain curves resulting from the simple strain deformations of the crystalline MDI/BDO atomistic model at constant deformation rate. Each part of Figure 3 describes the response of all six stress tensor elements as a function of one nonzero strain element, up to 10% true strain. The slopes of these curves in the limit of low strain correspond to the elements of the stiffness matrix **C**. By calculating the slopes of

tangential linear fits to these curves up to a true strain of 2%, the 36 stiffnesses were estimated.

A number of interesting features can be observed from the stress-strain plots of Figure 3. At low strains (< 2%), all of the stress-strain plots have finite slope, which is indicative of 36 finite stiffnesses. Of these 36 stiffnesses, only 21 are independent because of the triclinic symmetry of the MDI/BDO unit cell[52]; this symmetry is confirmed by these results. Secondly, at low strains ($0 < \varepsilon < 0.02$), the stress-strain dependence was practically linear and elastic, as confirmed by reversal of the strains.

Eq. 2 shows the complete stiffness matrix $\mathbf{C}_{crystal}$ obtained for the crystalline MDI/BDO at the slow deformation rate. The calculated stiffness matrix was found to be symmetric about the main diagonal and positive definite, having all of its eigenvalues strictly positive. This indicates that the system was mechanically stable. The inverses of the diagonal elements of the compliance tensor are the elastic moduli of the material, E_i, i=1,2,3 and G_{i-3}, i=4,5,6. These values are listed in Table 3, where applicable, based on the method used for their estimation.

$$C_{crystal} = \begin{bmatrix} 3.58 & 1.76 & 3.97 & -0.06 & -0.48 & 0.30 \\ & 3.53 & 3.00 & 0.11 & -0.27 & -0.69 \\ & & 20.82 & 0.63 & -0.29 & 0.73 \\ & & & 1.14 & -1.01 & 0.16 \\ & & & & 2.24 & -0.39 \\ & & & & & 2.61 \end{bmatrix} \quad (2)$$

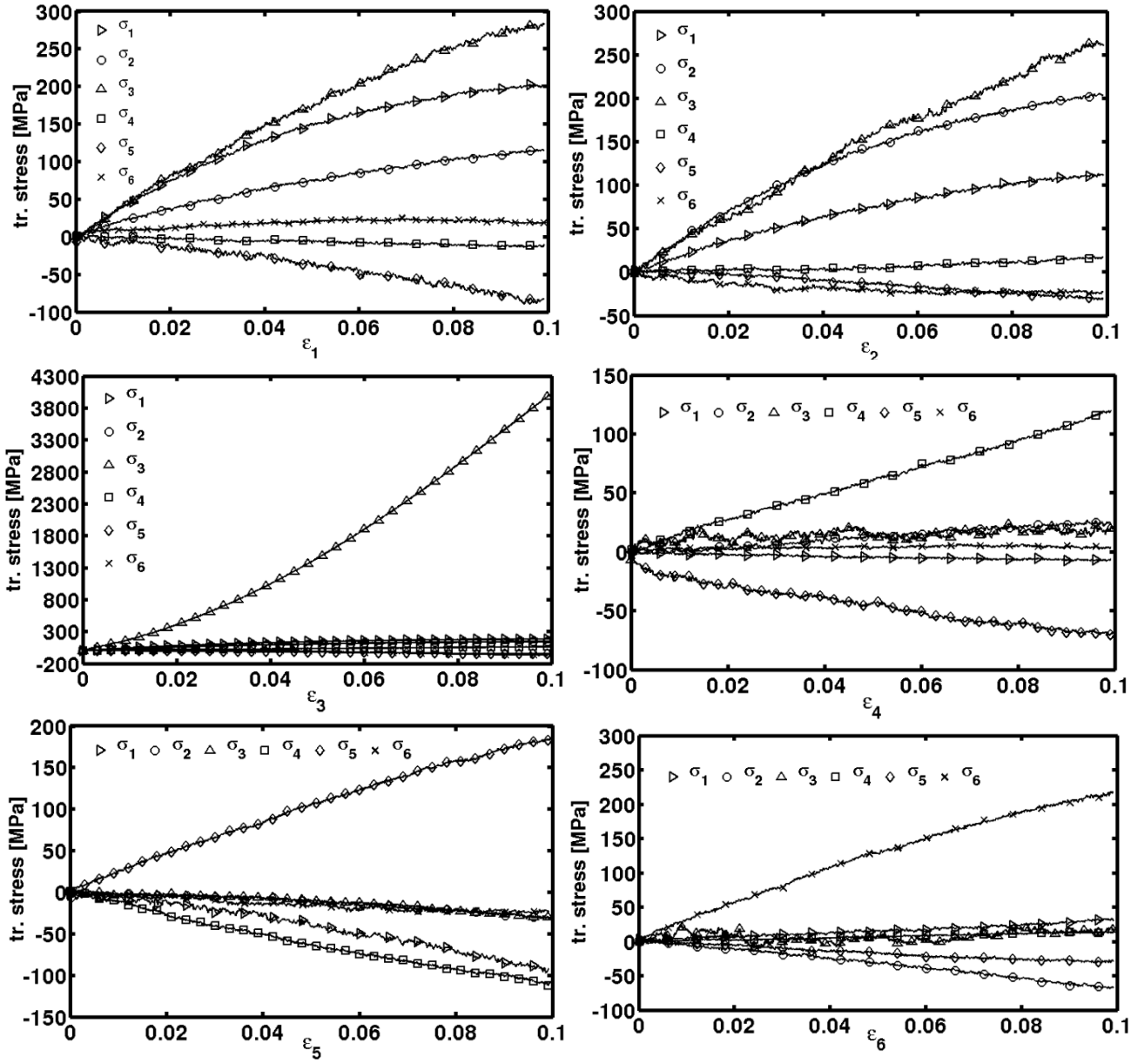

Figure 3: Linear-elastic stress strain behavior of crystalline MDI/BDO under simple straining (uniaxial and shear) at T = 300 K and P = 1 atm. The slopes of these plots, up to a true strain of 2%, were identified as the corresponding element of the stiffness matrix.

Table 3 shows that the elastic constants calculated by the two different deformation protocols are consistent. It also shows the anisotropic nature of crystalline MDI/BDO. The

stiffness along the chain direction (E_3) of crystalline MDI/BDO is almost 7 times larger than the stiffnesses in the other two principal directions, yet substantially smaller than the stiffness of crystalline polyethylene (PE) (E_3 ~ 283 GPa)[54] and PTMO (E_3 ~ 67 GPa)[53] when stretched along their chain directions. This is probably a consequence of the bent zigzag molecular conformation of the MDI/BDO chains in the chain direction (see Figure 1), which allows for easier extensibility compared to the linear all-trans conformations of PE and PTMO. This conformation imparts increased flexibility to the MDI/BDO crystal, which can then be translated to decreased stiffness along the chain direction. Contrary to that, the two lateral stiffnesses of the MDI/BDO crystal, E_1 and E_2, along with the corresponding shear moduli, G_i, i=1,2,3, are larger than the ones of crystalline PTMO[53], which is a consequence of the dense packing in the MDI/BDO crystal lattice opposing shear or lateral deformation. The isothermal compressibility of the MDI/BDO crystal (0.41 GPa^{-1}) is intermediate between that of crystalline PE (0.15 GPa^{-1}) [54] and crystalline (0.63 GPa^{-1}) PTMO[53].

Table 3: Basic mechanical properties calculated by NEMD for the MDI/BDO crystal at T = 300 K and P = 1 atm. Uncertainty in all elastic moduli is of the order of 0.05 GPa.

Crystal MDI/BDO		
Method / **Property**	**Simple strain**	**Uniaxial strain**
E_1, E_2, E_3 [GPa]	2.08, 2.29, 14.26	2.01, 2.32, 14.19
G_1, G_2, G_3 [GPa]	0.62, 1.20, 2.22	N/A
β_T [GPa^{-1}]	0.41	0.36

At intermediate strains ($0.02 < \varepsilon < 0.1$), the stress-strain plots of Figure 3 become nonlinear. Within this strain interval, there was no clear evidence of a yield point such as that typically observed in plastic deformation of amorphous polymers. Instead, a gradual rollover behavior was exhibited in most cases, indicative of strain-induced softening. The notable

exception to this behavior is the σ_3-ε_3 curve, which is significantly stiffer than the other curves and exhibits strain-induced hardening. We believe that the σ_3-ε_3 response is the result of loading the intramolecular degrees of freedom within the chains, which becomes increasingly resistant to deformation as the zigzag-shaped polymer chains become more extended and aligned with the strain direction. This is equivalent to an increase of the angle formed between the two consecutive phenyl rings (i.e., angle formed by atoms C11, C14 and C15) of the asymmetric unit shown in Figure 1(b). By contrast, the other responses are predominantly intermolecular in nature, controlled by van der Waals forces, and become softer as the density of the crystal declines with increasing strain. The lack of a clear yield point could be due, at least in part, to the absence of defects such as twists, jogs or chain ends within the simulation, which can act as stress concentrators for onset of plastic deformation.

5. Conclusions

In summary, we report the use of molecular simulations to study the structure and properties of the MDI/BDO crystal, as one of the major components of thermoplastic polyurethanes. For the first time, a molecular model of the MDI/BDO crystal was built, equilibrated and studied in atomistic detail. A united atom force field has been shown to capture accurately the inter- and intramolecular interactions for this system. The equilibrium crystal density and lattice parameters obtained by simulation compare favorably to experimental measurements. Further structural analysis of the model crystal revealed good agreement between the three-dimensional conformation of MDI/BDO chains in the crystal and existing experimental observations.

Analysis of deformation of the MDI/BDO crystal was also performed. The crystal is mechanically anisotropic, with reduced stiffness along the chain direction and intermediate compressibility compared to PE and PTMO crystals. This observation was attributed to the spatial arrangement and general conformation of the MDI/BDO chains in the crystal, which allow for increased extensibility along the chain direction. Contrary to that, the MDI/BDO

crystal showed increased stiffness when deformed lateral to the chain axis or when sheared. This behavior is attributed to the dense packing of chains in the crystal.

Using simple strain (uniaxial and shear) loading conditions, the overall stress-strain behavior up to a true strain of 10%, and therewith the entire stiffness matrix of the system, was obtained. Thus, the linear-elastic mechanical behavior of the crystal is quantified for the first time. Knowing the full stiffness matrix could facilitate the parameterization of micromechanical models and provide useful input for micromechanical homogenization processes for the study of composite systems that contain crystalline MDI/BDO as one of their constituent parts, such as thermoplastic polyurethanes.

Supporting Information

Appendix A: Fractional coordinates of all atoms in the crystalline MDI/BDO unit cell

Appendix B: Force field functional forms and parameters

Acknowledgement

We gratefully acknowledge BASF SE for financial support. We are also very grateful to Dr. Hansohl Cho for many stimulating discussions and for valuable suggestions concerning the deformation analysis.

References

[1] M. Szycher, Szycher's Handbook of Polyurethanes, First Edition, Taylor & Francis1999.
[2] C.S. Schollenberger, H. Scptt, G.R. Moore, Polyurethan VC, a Virtually Crosslinked Elastomer, Rubber Chemistry and Technology 35(3) (1962) 742-752, DOI: 10.5254/1.3539953.
[3] S.L. Cooper, A.V. Tobolsky, Properties of linear elastomeric polyurethanes, Journal of Applied Polymer Science 10(12) (1966) 1837-1844, DOI: 10.1002/app.1966.070101204.
[4] R. Bonart, X-ray investigations concerning the physical structure of cross-linking in segmented urethane elastomers, Journal of Macromolecular Science, Part B 2(1) (1968) 115-138, DOI: 10.1080/00222346808212867.
[5] R. Bonart, Segmentierte Polyurethane, Die Angewandte Makromolekulare Chemie 58(1) (1977) 259-297, DOI: 10.1002/apmc.1977.050580112.

[6] R. Bonart, L. Morbitzer, G. Hentze, X-ray investigations concerning the physical structure of cross-linking in urethane elastomers. II. Butanediol as chain extender, Journal of Macromolecular Science, Part B 3(2) (1969) 337-356, DOI: 10.1080/00222346908205099.
[7] R. Bonart, L. Morbitzer, E.H. Müller, X-ray investigations concerning the physical structure of crosslinking in urethane elastomers. III. Common structure principles for extensions with aliphatic diamines and diols, Journal of Macromolecular Science, Part B 9(3) (1974) 447-461, DOI: 10.1080/00222347408204548.
[8] R. Bill, M. Dröscher, G. Wegner, Oligo(oxytetramethylene)s and their derivatives: Models for segmented poly(ether ester)s and polyurethanes, Die Makromolekulare Chemie 179(12) (1978) 2993-2996, DOI: 10.1002/macp.1978.021791220.
[9] J. Blackwell, K.H. Gardner, Structure of the hard segments in polyurethane elastomers, Polymer 20(1) (1979) 13-17, DOI: http://dx.doi.org/10.1016/0032-3861(79)90035-1.
[10] J. Ferguson, D.J. Hourston, R. Meredith, D. Patsavoudis, Mechanical relaxations in a series of polyurethanes with varying hard to soft segment ratio, European Polymer Journal 8(3) (1972) 369-383, DOI: http://dx.doi.org/10.1016/0014-3057(72)90102-4.
[11] D.S. Huh, S.L. Cooper, Dynamic mechanical properties of polyurethane block polymers, Polymer Engineering & Science 11(5) (1971) 369-376, DOI: 10.1002/pen.760110504.
[12] C.S.P. Sung, T.W. Smith, C.B. Hu, N.-H. Sung, Hysteresis Behavior in Polyether Poly(urethaneureas) Based on 2,4-Toluene Diisocyanate, Ethylenediamine, and Poly(tetramethylene oxide), Macromolecules 12(3) (1979) 538-540, DOI: 10.1021/ma60069a043.
[13] C.E. Wilkes, C.S. Yusek, Investigation of domain structure in urethan elastomers by X-Ray and thermal methods, Journal of Macromolecular Science, Part B 7(1) (1973) 157-175, DOI: 10.1080/00222347308212578.
[14] J. Blackwell, M. Ross, X-ray studies of the structure of polyurethane hard segments, Journal of Polymer Science: Polymer Letters Edition 17(7) (1979) 447-451, DOI: 10.1002/pol.1979.130170709.
[15] J. Blackwell, M.R. Nagarajan, T.B. Hoitink, Structure of polyurethane elastomers. X-ray diffraction and conformational analysis of MDI-propandiol and MDI-ethylene glycol hard segments, Polymer 22(11) (1981) 1534-1539, DOI: http://dx.doi.org/10.1016/0032-3861(81)90325-6.
[16] J. Blackwell, M.R. Nagarajan, T.B. Hoitink, Structure of polyurethane elastomers: effect of chain extender length on the structure of MDI/diol hard segments, Polymer 23(7) (1982) 950-956, DOI: http://dx.doi.org/10.1016/0032-3861(82)90392-5.
[17] L. Born, J. Crone, H. Hespe, E.H. Müller, K.H. Wolf, On the structure of polyurethane hard segments based on MDI and butanediol-1,4: X-ray diffraction analysis of oriented elastomers and of single crystals of a model compound, Journal of Polymer Science: Polymer Physics Edition 22(2) (1984) 163-173, DOI: 10.1002/pol.1984.180220202.
[18] C.W. Patterson, D. Hanson, A. Redondo, S.L. Scott, N. Henson, Conformational analysis of the crystal structure for MDI/BDO hard segments of polyurethane elastomers, Journal of Polymer Science Part B: Polymer Physics 37(17) (1999) 2303-2313, DOI: 10.1002/(SICI)1099-0488(19990901)37:17<2303::AID-POLB2>3.0.CO;2-O.
[19] S. Abouzahr, G.L. Wilkes, Z. Ophir, Structure-property behaviour of segmented polyether-MDI-butanediol based urethanes: effect of composition ratio, Polymer 23(7) (1982) 1077-1086, DOI: http://dx.doi.org/10.1016/0032-3861(82)90411-6.
[20] R.M. Briber, E.L. Thomas, Investigation of two crystal forms in MDI/BDO-based polyurethanes, Journal of Macromolecular Science, Part B 22(4) (1983) 509-528, DOI: 10.1080/00222348308224773.
[21] R.M. Briber, E.L. Thomas, The structure of MDI/BDO-based polyurethanes: Diffraction studies on model compounds and oriented thin films, Journal of Polymer Science: Polymer Physics Edition 23(9) (1985) 1915-1932, DOI: 10.1002/pol.1985.180230913.
[22] A.L. Chang, R.M. Briber, E.L. Thomas, R.J. Zdrahala, F.E. Critchfield, Morphological study of the structure developed during the polymerization of a series of segmented polyurethanes, Polymer 23(7) (1982) 1060-1068, DOI: http://dx.doi.org/10.1016/0032-3861(82)90409-8.

[23] K.W. Chau, P.H. Geil, Domain morphology in polyurethanes, Polymer 26(4) (1985) 490-500, DOI: http://dx.doi.org/10.1016/0032-3861(85)90147-8.
[24] Z.S. Petrović, J. Ferguson, Polyurethane elastomers, Progress in Polymer Science 16(5) (1991) 695-836, DOI: http://dx.doi.org/10.1016/0079-6700(91)90011-9.
[25] S. Plimpton, Fast Parallel Algorithms for Short-Range Molecular Dynamics, Journal of Computational Physics 117(1) (1995) 1-19, DOI: http://dx.doi.org/10.1006/jcph.1995.1039.
[26] R.J. Zdrahala, R.M. Gerkin, S.L. Hager, F.E. Critchfield, Polyether-based thermoplastic polyurethanes. I. Effect of the hard-segment content, Journal of Applied Polymer Science 24(9) (1979) 2041-2050, DOI: 10.1002/app.1979.070240912.
[27] B. Chen, J.J. Potoff, J.I. Siepmann, Monte Carlo Calculations for Alcohols and Their Mixtures with Alkanes. Transferable Potentials for Phase Equilibria. 5. United-Atom Description of Primary, Secondary, and Tertiary Alcohols, The Journal of Physical Chemistry B 105(15) (2001) 3093-3104, DOI: 10.1021/jp003882x.
[28] C. Chen, P. Depa, V.G. Sakai, J.K. Maranas, J.W. Lynn, I. Peral, J.R.D. Copley, A comparison of united atom, explicit atom, and coarse-grained simulation models for poly(ethylene oxide), The Journal of Chemical Physics 124(23) (2006) 234901, DOI: doi:http://dx.doi.org/10.1063/1.2204035.
[29] K.A. Maerzke, N.E. Schultz, R.B. Ross, J.I. Siepmann, TraPPE-UA Force Field for Acrylates and Monte Carlo Simulations for Their Mixtures with Alkanes and Alcohols, The Journal of Physical Chemistry B 113(18) (2009) 6415-6425, DOI: 10.1021/jp810558v.
[30] J.M. Stubbs, J.J. Potoff, J.I. Siepmann, Transferable Potentials for Phase Equilibria. 6. United-Atom Description for Ethers, Glycols, Ketones, and Aldehydes, The Journal of Physical Chemistry B 108(45) (2004) 17596-17605, DOI: 10.1021/jp049459w.
[31] C.D. Wick, J.M. Stubbs, N. Rai, J.I. Siepmann, Transferable Potentials for Phase Equilibria. 7. Primary, Secondary, and Tertiary Amines, Nitroalkanes and Nitrobenzene, Nitriles, Amides, Pyridine, and Pyrimidine, The Journal of Physical Chemistry B 109(40) (2005) 18974-18982, DOI: 10.1021/jp0504827.
[32] C.D. Wick, M.G. Martin, J.I. Siepmann, Transferable Potentials for Phase Equilibria. 4. United-Atom Description of Linear and Branched Alkenes and Alkylbenzenes, The Journal of Physical Chemistry B 104(33) (2000) 8008-8016, DOI: 10.1021/jp001044x.
[33] J.M. Briggs, T.B. Nguyen, W.L. Jorgensen, Monte Carlo simulations of liquid acetic acid and methyl acetate with the OPLS potential functions, The Journal of Physical Chemistry 95(8) (1991) 3315-3322, DOI: 10.1021/j100161a065.
[34] E.M. Duffy, P.J. Kowalczyk, W.L. Jorgensen, Do denaturants interact with aromatic hydrocarbons in water?, Journal of the American Chemical Society 115(20) (1993) 9271-9275, DOI: 10.1021/ja00073a050.
[35] W.L. Jorgensen, J.M. Briggs, M.L. Contreras, Relative partition coefficients for organic solutes from fluid simulations, The Journal of Physical Chemistry 94(4) (1990) 1683-1686, DOI: 10.1021/j100367a084.
[36] W.L. Jorgensen, E.R. Laird, T.B. Nguyen, J. Tirado-Rives, Monte Carlo simulations of pure liquid substituted benzenes with OPLS potential functions, Journal of Computational Chemistry 14(2) (1993) 206-215, DOI: 10.1002/jcc.540140208.
[37] W.L. Jorgensen, J.D. Madura, C.J. Swenson, Optimized intermolecular potential functions for liquid hydrocarbons, Journal of the American Chemical Society 106(22) (1984) 6638-6646, DOI: 10.1021/ja00334a030.
[38] W.L. Jorgensen, D.S. Maxwell, J. Tirado-Rives, Development and Testing of the OPLS All-Atom Force Field on Conformational Energetics and Properties of Organic Liquids, Journal of the American Chemical Society 118(45) (1996) 11225-11236, DOI: 10.1021/ja9621760.
[39] W.L. Jorgensen, D.L. Severance, Aromatic-aromatic interactions: free energy profiles for the benzene dimer in water, chloroform, and liquid benzene, Journal of the American Chemical Society 112(12) (1990) 4768-4774, DOI: 10.1021/ja00168a022.

[40] W.L. Jorgensen, J. Tirado-Rives, The OPLS [optimized potentials for liquid simulations] potential functions for proteins, energy minimizations for crystals of cyclic peptides and crambin, Journal of the American Chemical Society 110(6) (1988) 1657-1666, DOI: 10.1021/ja00214a001.
[41] G.A. Kaminski, R.A. Friesner, J. Tirado-Rives, W.L. Jorgensen, Evaluation and Reparametrization of the OPLS-AA Force Field for Proteins via Comparison with Accurate Quantum Chemical Calculations on Peptides†, The Journal of Physical Chemistry B 105(28) (2001) 6474-6487, DOI: 10.1021/jp003919d.
[42] S.J. Weiner, P.A. Kollman, D.A. Case, U.C. Singh, C. Ghio, G. Alagona, S. Profeta, P. Weiner, A new force field for molecular mechanical simulation of nucleic acids and proteins, Journal of the American Chemical Society 106(3) (1984) 765-784, DOI: 10.1021/ja00315a051.
[43] W.L. Jorgensen, C.J. Swenson, Optimized intermolecular potential functions for amides and peptides. Structure and properties of liquid amides, Journal of the American Chemical Society 107(3) (1985) 569-578, DOI: 10.1021/ja00289a008.
[44] W.L. Jorgensen, Optimized intermolecular potential functions for liquid alcohols, The Journal of Physical Chemistry 90(7) (1986) 1276-1284, DOI: 10.1021/j100398a015.
[45] W.L. Jorgensen, J.M. Briggs, Monte Carlo simulations of liquid acetonitrile with a three-site model, Molecular Physics 63(4) (1988) 547-558, DOI: 10.1080/00268978800100371.
[46] W.C. Swope, H.C. Andersen, P.H. Berens, K.R. Wilson, A computer simulation method for the calculation of equilibrium constants for the formation of physical clusters of molecules: Application to small water clusters, The Journal of Chemical Physics 76(1) (1982) 637-649, DOI: doi:http://dx.doi.org/10.1063/1.442716.
[47] W.G. Hoover, Canonical dynamics: Equilibrium phase-space distributions, Physical Review A 31(3) (1985) 1695-1697, DOI.
[48] S. Nosé, A unified formulation of the constant temperature molecular dynamics methods, The Journal of Chemical Physics 81(1) (1984) 511-519, DOI: doi:http://dx.doi.org/10.1063/1.447334.
[49] N. Lempesis, P.J. in ‘t Veld, G.C. Rutledge, Atomistic Simulation of the Structure and Mechanics of a Semicrystalline Polyether, Macromolecules 49(15) (2016) 5714-5726, DOI: 10.1021/acs.macromol.6b00555.
[50] R.G.C. Arridge, Mechanics of Polymers, Clarendon Press1975.
[51] I.M. Ward, J. Sweeney, An Introduction to the Mechanical Properties of Solid Polymers, Wiley2004.
[52] J.F. Nye, Physical Properties of Crystals: Their Representation by Tensors and Matrices, Clarendon Press1985.
[53] N. Lempesis, P.J. In 't Veld, G.C. Rutledge, Atomistic simulation of the structure and mechanics of a semicrystalline polyether, Macromolecules in press (2016), DOI.
[54] D.J. Lacks, G.C. Rutledge, Simulation of the temperature dependence of mechanical properties of polyethylene, The Journal of Physical Chemistry 98(4) (1994) 1222-1231, DOI: 10.1021/j100055a030.